ACS SENSORS

pubs.acs.org/acssensors

Article

Preparation of BiOI-Functionalized ZnO Nanorods for Ppb-Level NO_2 Detection at Room Temperature

Yueyue Li, Yuanzhen Liu, Yi Lu, Ziqi Liu, Chengming Sui, Yilin Wang, Lin Yang, Fengmin Liu,* Peng Sun, Fangmeng Liu, and Geyu Lu*

Cite This: *ACS Sens.* 2022, 7, 3915−3922

Read Online

ACCESS | Metrics & More | Article Recommendations | Supporting Information

ABSTRACT: Light activation is an effective method to improve sensor performance at room temperature (RT). This work realized the effective detection of trace-level NO_2 at RT under visible light by combining ZnO with the excellent photocatalyst BiOI. A 1.5 atom % BiOI−ZnO-based sensor under 520 nm light exhibited optimal sensing properties with the maximum responses (13.9 to 1 ppm NO_2), fast response/recovery time (66 s/47 s to 1 ppm), and a low detection limit of 25 ppb (theoretically 0.34 ppb). In the meantime, the sensor also possessed excellent selectivity, repeatability, and stability. The excellent properties were attributed to the high concentration of oxygen vacancies and the prolonged lifetime of photogenerated carriers. In addition, the observed photovoltaic effect of the sensor at RT indicated that the sensor held application prospects in the photovoltaic self-power field.

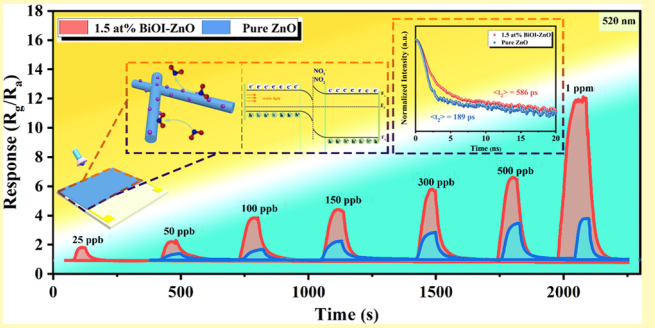

KEYWORDS: *ZnO nanorods, BiOI, NO_2 sensor, visible light, Low detection limit, fast speeds*

Nitrogen oxides (NO_x), mainly from industrial emissions, vehicle exhaust, and natural gas burning,[1,2] have been one of the major air pollutants. NO_x can cause chronic respiratory disease, asthma attacks, and even lung cancer in both children and adults.[1] Recently, researchers have also found a positive correlation between ppb-level NO_2 in urban air pollution and the mortality of COVID-19.[3] Consequently, it is of great importance to monitor NO_2 in the environment.

Metal oxide semiconductor (MOS)-based chemiresistive gas sensors, such as SnO_2, ZnO, WO_3, and Fe_2O_3, exhibit excellent properties in detecting NO_2.[4−7] However, they usually need to work at high temperatures (150−400 °C) for obtaining enough thermal energy to overcome the activation energy barrier and complete the surface redox reaction. High working temperatures decrease the stability and lifetime of the sensors, bring potential safety hazards in the presence of flammable and explosive gases, and are also inconducive to the integration of devices.[8−10] Till now, great efforts have been devoted to explore MOS-based sensors operating at room temperature (RT) by adopting methods such as adding conductive polymers, doping noble metals, and constructing heterojunctions.[11−13] These methods effectively improve the sensors' response at RT, but there is still the problem of slow gas adsorption/desorption speeds. Light excitation is an effective way to solve this problem due to photogenerated carriers, which will effectively improve the conductivity of sensors and enhance the activity of the surface reaction. ZnO has gained widespread attention due to both outstanding photoelectronic and gas-sensing properties. Among a variety of morphologies, ZnO nanorods (NRs), having the unique advantages of low defect density, good crystallinity, and large grain sizes, often exhibit better sensing properties such as rapid response/recovery speeds.[14] However, the wide band gap of ZnO results in a narrow light absorption range. To enlarge the absorption wavelength of the material to improve the utilization of light energy, it is an effective and facile strategy to combine ZnO with other suitable photocatalysts to construct heterojunctions.

Ternary oxide semiconductors, BiOX (X = F, Cl, Br, and I), are promising catalysts, as they are nontoxic and inexpensive and have an environmentally friendly nature. BiOX are composed of $Bi_2O_2^{2+}$ layers with a layered structure interleaved by slabs of halide atoms. Such a unique layered structure with excellent photoelectronic properties under visible light results in widespread application in the fields of photocatalysis, solar cells, and photoelectric detectors.[15−17] Among BiOX, BiOI has the narrowest band gap and exhibits higher light catalytic activity.[18] Taking advantage of this feature, BiOI has great potential to be a good photosensitizer in the gas sensor field.

Received: September 12, 2022
Accepted: November 15, 2022
Published: November 23, 2022

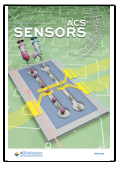

Unfortunately, relevant studies have not been reported at present.

In this work, we investigated the improvement effect of illumination on the NO_2 sensing performance of sensors based on BiOI-functionalized ZnO at RT. The characteristics of composites and sensing properties of sensors to NO_2 under excitation of different wavelengths at RT were tested and discussed in detail. What's more, the gas-sensing mechanism was analyzed using the gas molecules adsorption model.

EXPERIMENTAL SECTION

Gas Sensor Fabrication. The synthesis methods of pure ZnO, pure BiOI, and BiOI−ZnO were described in the Supporting information. In total, 10 mg of samples were mixed with ethanol and then covered onto Al_2O_3 substrates (10 mm × 10 mm) with Au interdigital electrodes (15 pairs, and 50 μm between each pair of electrodes). The brushed substrates were dried in an 80 °C oven and then annealed for 1 h under an Ar atmosphere at 300 °C with a rate of 10 °C/min. The whole process of fabrication is presented in Figure 1.

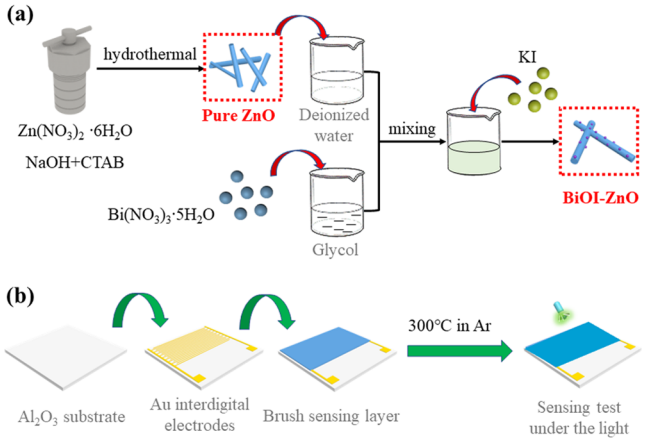

Figure 1. Diagrams of (a) BiOI−ZnO preparation and (b) sensor fabrication.

Gas Sensor Measurement. The sensing performances were evaluated through a static method consistent with the published paper[19] (the more detailed information is in the Supporting information).

RESULTS AND DISCUSSION

Morphology and Structure Characterization. In XRD patterns shown in Figure 2a, pure ZnO was completely in accordance with the standard PDF card (No. 76-0704), and no additional peaks were observed in the composites (1.0−3.0 atom % BiOI−ZnO), which was due to the low contents of BiOI. In fact, pure BiOI in Figure S1 can be indexed with the standard PDF card (No. 73-2062). When the content was increased to 10.0−15.0 atom %, a new peak belonging to the (012) plane of BiOI was observed at about 28.26° in Figure S1, indicating the existence of BiOI crystals in the composites.[20] Besides, it can be seen that the peak position of the (012) plane in BiOI−ZnO was slightly shifted to the left compared with pure BiOI due to the influence of tensile stress from the ZnO crystal.[21]

Figure 2b,c displays the microstructure of pure ZnO and BiOI. Pure ZnO exhibited a nanorod shape with a smooth surface, and pure BiOI microballs were formed by stacking thin nanosheets. Figure 2d shows that 1.5 atom % BiOI was attached to the surface of ZnO after its addition, making the ZnO surface no longer smooth. In Figure 2e,f, the composite was further examined by TEM and HRTEM, and lattice fringes with spacings of 0.33 and 0.28 nm were observed, corresponding to the (012) plane of BiOI and the (100) plane of ZnO, respectively. In addition, the mapping results shown in Figure 2g−j revealed elements including Zn, O, Bi, and I in the BiOI−ZnO composite, indicating that the BiOI crystals were equally dispersed throughout the surface of ZnO.

The Raman spectra are displayed in Figure 3a. The high-intensity peaks at ∼438.36 cm^{-1} were Raman-active E_2 modes, which were related to the crystalline hexagonal wurtzite structure of ZnO samples, and the peak at ∼233.02 cm^{-1} was derived from the surface phonon mode of the nanostructure.[22,23] With the increase of BiOI contents, a peak appeared at 147.72 cm^{-1} in 3.0 atom % BiOI−ZnO due to the E_g internal Bi−I stretching mode.[24] FTIR was also employed to learn more about chemical bonding on the surface of samples (Figures 3b and S2). The characteristic peak of pure ZnO, attributed to the stretching of the Zn−O bond, was located at 528.09 cm^{-1}, but the position of this peak in composites tended to weaken and broaden with the increasing amounts of BiOI due to the Bi−O bond at 485.03 cm^{-1}.[25,26] The results of Raman and FTIR both proved the formation of BiOI crystals on ZnO NRs.

The absorption band edges of all samples can be seen in UV−vis adsorption spectra in Figure 3c. Pure ZnO exhibited strong absorption in the UV region, while pure BiOI exhibited at around 625 nm in the visible light region. For the composites, the adsorption extended to the visible light region when the content of BiOI exceeded 1.5 atom %.[19] The optical band gaps of pure ZnO and pure BiOI were, respectively, determined to be 3.19 and 1.98 eV according to the converted Tauc curves shown in Figure 3d. The band gaps of composites were all narrower than that of ZnO, and decreased gradually with the increase of BiOI contents, indicating more defects were produced in the composites.[25−27]

XPS was conducted to further explore the elements' chemical states. The survey scan of pure ZnO and the BiOI−ZnO composites in Figure S3a showed all elements' information. Figure S3b presents the two peaks of Zn 2p, which were both situated at approximately 1044.0 and 1020.9 eV in all samples. The three peaks of O 1s shown in Figure 3e were attributed to the lattice oxygen (O_L), oxygen vacancies (O_V), the chemisorbed oxygen (O_C, from CO_2 and H_2O), and the oxygen in the Bi−O bond (O_{Bi}).[21,28] The ratios of O_V in ZnO and the composites are shown in Table S1, and 1.5 atom % BiOI−ZnO had the highest content. The existence of the highest content indicated that BiOI can not only cover the surface during the in situ growth on ZnO to reduce the exposure of surface defects but also induced more defects on the ZnO surface simultaneously. Moreover, the peak of O_{Bi} increased with the increasing content of BiOI in the composites. Additionally, Figure S3c,d depicts the results of Bi 4f and I 3d. The XPS results further confirmed the composition of BiOI in ZnO.

Gas-Sensing Properties. According to the optical band gap of the materials, four different lights with wavelengths of 365, 460, 490, and 520 nm were selected to study the effect on the sensors' performances. The specific base resistances of the sensors under different light wavelengths are recorded in Figure 4a. The resistance of pure ZnO was the smallest, and those of composites gradually increased with the increase of BiOI contents due to the more formed heterojunctions. Taking

https://doi.org/10.1021/acssensors.2c01988
ACS Sens. 2022, 7, 3915−3922

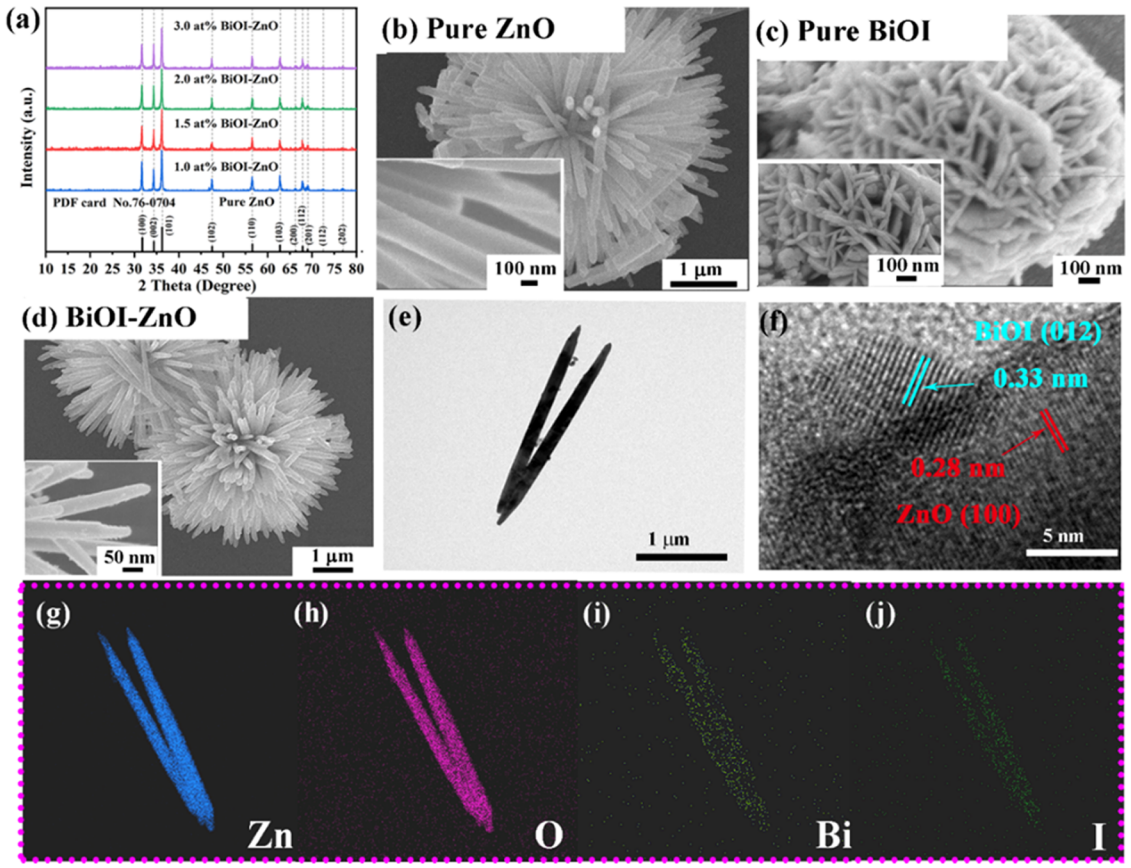

Figure 2. (a) XRD patterns of materials; (b–d) the SEM pictures (the insets were the magnified details); (e–f) the TEM pictures of 1.5 atom % BiOI–ZnO and the lattice fringes; and (g–j) the mapping results including Zn, O, Bi, and I.

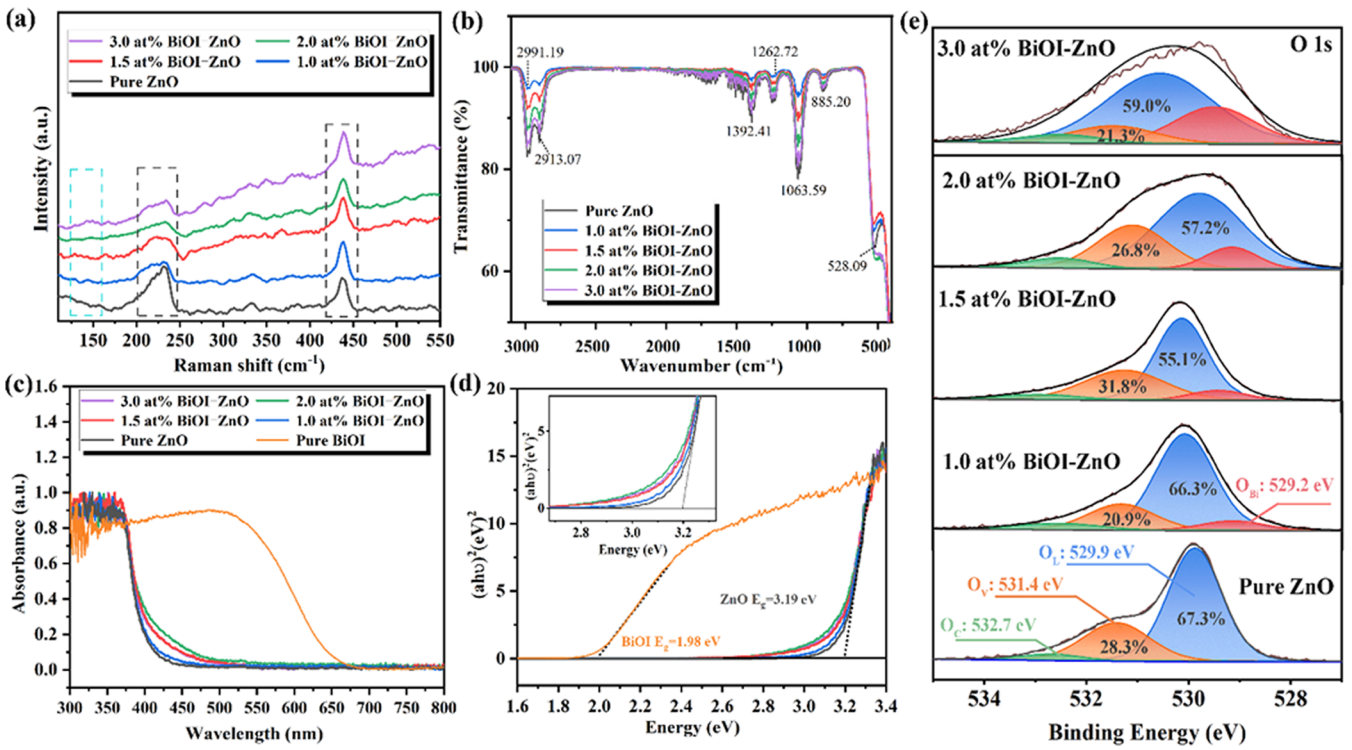

Figure 3. (a) Raman spectra, (b) FTIR spectra, (c) UV–vis adsorption spectra, and (d) Tauc plots of all samples. (e) O 1s from the XPS spectra of pure ZnO and BiOI–ZnO composites.

https://doi.org/10.1021/acssensors.2c01988
ACS Sens. 2022, 7, 3915–3922

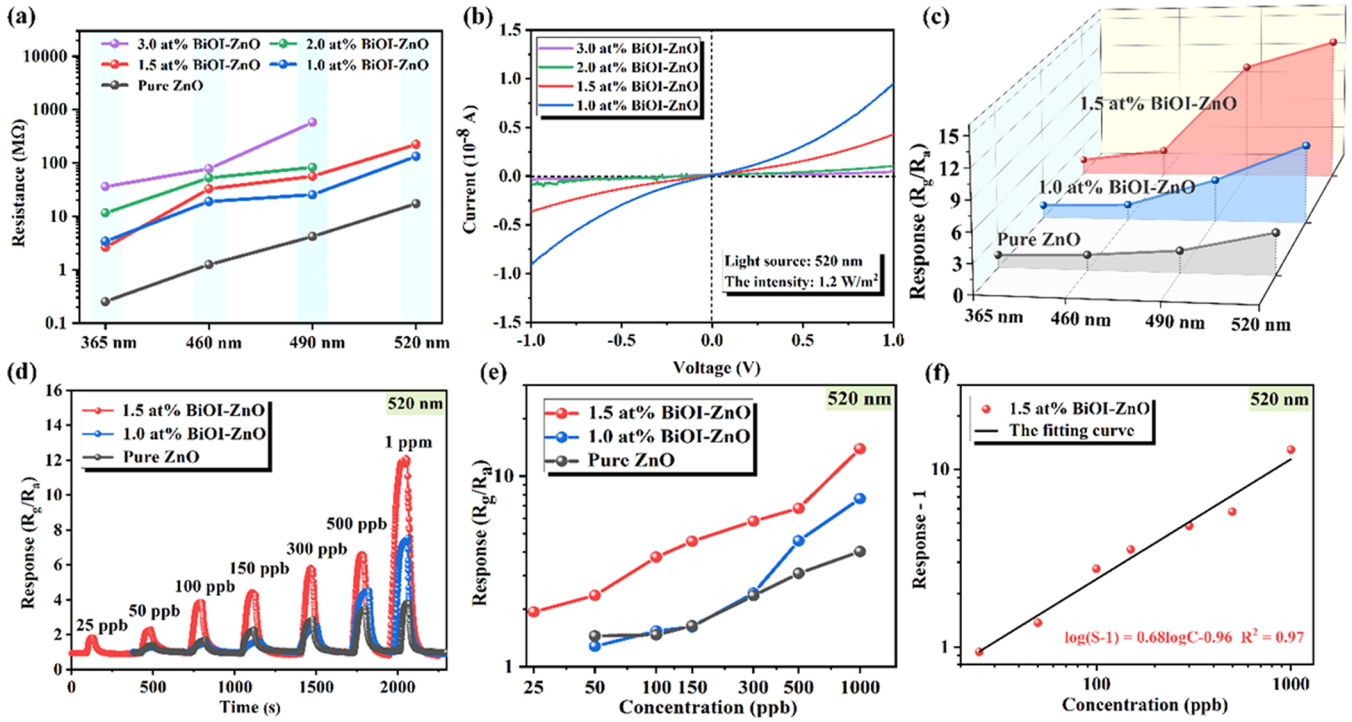

Figure 4. (a) Initial resistance of materials under different lights; (b) the $I-V$ curves under 520 nm light; (c) the response of sensors to 1 ppm NO_2; (d, e) the response curves and the comparison under 520 nm light; and (f) the linear fitting curve of the 1.5 atom % BiOI−ZnO responses.

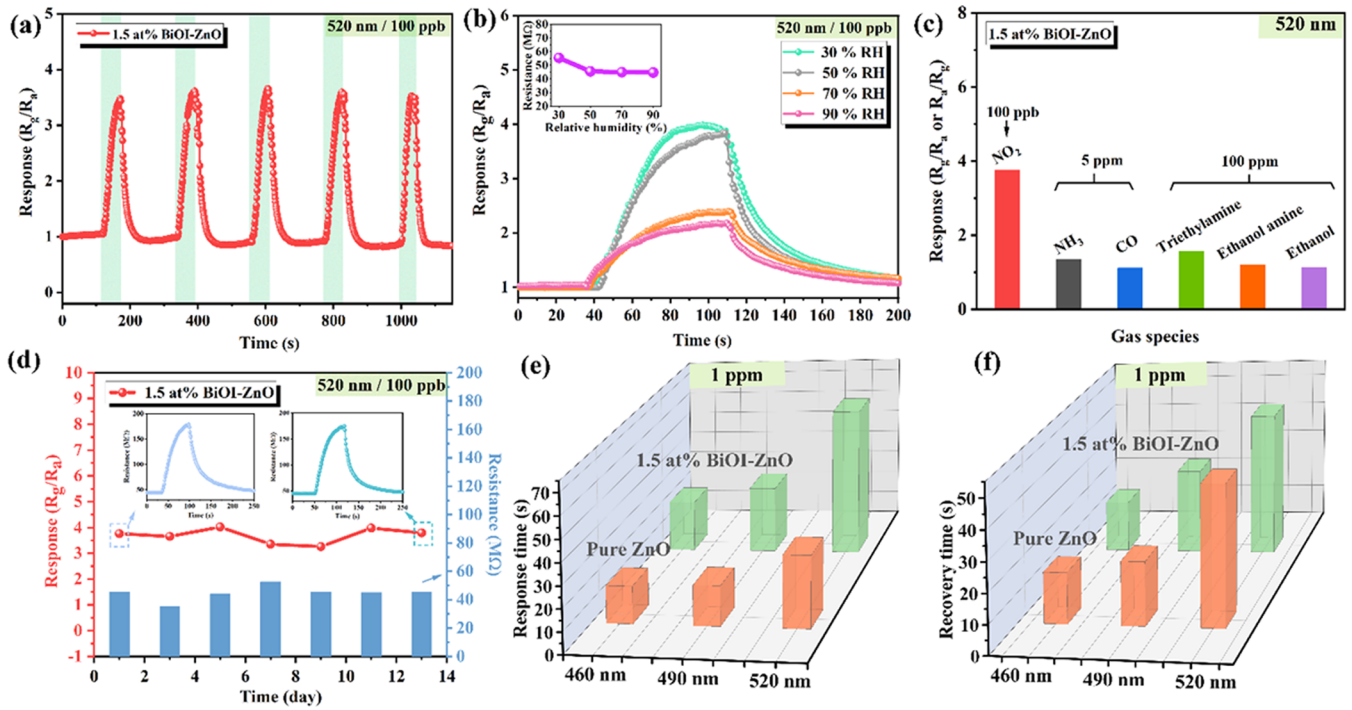

Figure 5. (a) Repeatability; (b) response curves under different humidities; (c) selectivity; (d) stability during two weeks of the 1.5 atom % BiOI−ZnO-based sensor; and (e, f) response/recovery times of sensors to 1 ppm NO_2 under different lights.

the situation under 520 nm as an example, the variation trends of resistance were consistent with the findings of $I-V$ curves, as shown in Figure 4b. Moreover, the $I-V$ curves of BiOI−ZnO composites also exhibited the rectifying property, which demonstrated the formation of a heterojunction between BiOI and ZnO.[29] In addition, Figure S4 also revealed the poorest conductivity of pure BiOI. In contrast, the resistance of the sensors in the dark was too large to be detected, demonstrating the difficulty to further explore the sensors' properties in the dark.

The sensing performances of all sensors were investigated under different wavelength lights. Figure S5a,b reveals the poor sensitivity of sensors to 1−5 ppm NO_2 under 365 nm light. The sensitivities of these sensors were improved after exposure

https://doi.org/10.1021/acssensors.2c01988
ACS Sens. 2022, 7, 3915−3922

to 460 nm light. As shown in Figure S5c,d, the responses of the sensors based on 1.0 and 1.5 atom % BiOI−ZnO increased compared with that of pure ZnO, but those of 2.0 and 3.0 atom % BiOI−ZnO decreased due to the excessive addition of BiOI. In comparison to pure ZnO, the improved responses of the sensors based on BiOI−ZnO composites were due to the higher visible light absorption, the increasing content of O_V, and the prolonged lifetime of carriers caused by the formed heterojunctions. However, too high content of BiOI gradually covered the surface active sites of ZnO to prevent gas adsorption, resulting in a bad sensing response. For sensors based on pure ZnO and 1.0 and 1.5 atom % BiOI−ZnO, the effect of extending the excitation wavelength on their sensing performance was further investigated. As presented in Figure 4c, the responses of the sensors to 1 ppm NO_2 increased with the increase of excitation light wavelength, which means that the lower detection limits of the sensors were expected to be further reduced under the excitation of 490 and 520 nm light. Figure S6 depicts the properties of three sensors to 0.1−1 ppm NO_2 under 490 nm illumination, in which the sensor based on 1.5 atom % BiOI−ZnO showed optimal NO_2 sensitivity. In Figure 4d,e, the responses of the sensors under 520 nm light further increased, and the highest responses were still seen at 1.5 atom % BiOI−ZnO. Surprisingly, the low detecting limit (LOD) was further lowered to 25 ppb for the 1.5 atom % BiOI−ZnO-based sensor. The above results indicated that the sensor based on 1.5 atom % BiOI−ZnO exhibited the best performance under 520 nm light. Figure 4f further presents the fitted relationship between the responses (S) and the NO_2 concentrations (C) in 0.025−1 ppm, which was consistent with the empirical law of gas adsorption.[30]

$$\log(S-1) = a\log(C) + b \tag{1}$$

The theoretical LOD could be deduced to 0.34 ppb according to the formula LOD = 3 × RMS_{noise}/slope (RMS_{noise} was 0.076, represented the root mean square of noise, which was the standard deviation of 30 experimental basic resistance in the test chamber).

Other gas-sensing properties of 1.5 atom % BiOI−ZnO under 520 nm light were further investigated. The repeatability is performed, as shown in Figure 5a, and the responses remained remarkably consistent over the course of five consecutive tests. Humidity was one of the main interference factors for sensors working at RT, and the properties under different humidities (30, 50, 70, and 90% RH) are explored in Figure 5b. The responses of the sensor to 100 ppb NO_2 decreased a lot under 70 and 90% RH, while the sensor could still meet the detection of ppb-level NO_2 under higher humidity. In addition, Figure 5c illustrates the selectivity of the sensor. The responses to CO, ethanol, and some gases containing nitrogen (NH_3, triethylamine, and ethanolamine) were all much lower, showing excellent selectivity to NO_2. The long-term stability of the sensor during two weeks is recorded in Figure 5d, and the insets show the resistance curves on the first day and the day after two weeks of continuous operation. Both the base resistance and response to 100 ppb NO_2 fluctuated slightly during the test period, indicating the good stability of the sensor. Table S2 lists and compares the properties of sensors based on ZnO in published works, and the sensor developed in this work held advantages in response/recovery speed. In fact, we also found a detrimental effect of 520 nm light on the response/recovery time of the 1.5 atom % BiOI−ZnO-based sensor, as shown in Figure 5e,f, which will be explained in the subsequent mechanism section.

Gas-Sensing Mechanism. The mechanism can be analyzed according to the gas adsorption/desorption model on the surface of N-type semiconductors. ZnO with an NR structure holds the advantages of low defect density, good crystallinity, and large grain sizes, resulting in a thin depletion layer and fast electron transfer.[14] On the surface of ZnO, some unpaired electrons are formed due to the presence of O_V, which provide reaction active sites for gas adsorption. When the sensor is placed in the air, O_2 is adsorbed on O_V to form a chemical adsorption state by capturing electrons, mainly including O_2^- at RT. Meanwhile, a depletion layer is formed on the surface, resulting in increased resistance. The reaction is as follows:

$$O_{2(ads)} + e^- \rightarrow O^-_{2(ads)} \tag{2}$$

Under light irradiation, electrons in the valence band (VB) absorb photon energy to transition to the conduction band (CB). More active photocarriers not only significantly improved the conductivity of the sensing material but also participated in the surface reaction.

$$h\upsilon \rightarrow e^-_{(h\upsilon)} + h^+_{(h\upsilon)} \tag{3}$$

$$O_{2(ads)} + e^-_{(h\upsilon)} \rightarrow O^-_{2(h\upsilon)} \tag{4}$$

When the sensor is in a NO_2 atmosphere, NO_2 adsorbed on the surface of ZnO not only directly captures $e^-_{(h\upsilon)}$ from CB but also reacts with $O_2^-{}_{(h\upsilon)}$. The generated NO_2^- obviously deepen the depletion layer so that leads to higher resistance.

$$NO_{2(ads)} + e^-_{(h\upsilon)} \rightarrow NO^-_{2(ads)} \tag{5}$$

$$NO_{2(ads)} + O^-_{2(h\upsilon)} \rightarrow NO^-_{2(ads)} + O_{2(gas)} \tag{6}$$

However, some of NO_2^- is reoxidized to NO_2 and desorbed from the surface under the action of $h^+_{(h\upsilon)}$.

$$NO^-_{2(ads)} + h^+_{(h\upsilon)} \rightarrow NO_{2(ads)} \tag{7}$$

When the adsorption/desorption process reaches equilibrium, the resistance of the sensor reaches a stable state. In fact, illumination can simultaneously affect the gas adsorption/desorption rates. From the entire process, it can be concluded that the responses can be greatly improved by increasing the proportion of surface O_V and accelerating the surface charge transfer rate. Therefore, for the BiOI−ZnO-based sensor, the enhanced change of responses was observed with the increase of the light wavelength. However, an inhibited effect was exhibited on the response/recovery speeds, shown in Figure 5e,f, due to the existence of equilibrium and the different photon energy. Short-wavelength (high photon energy) lights induce more photogenerated carriers in the sensing material, accelerating the dynamic equilibrium process and the response/recovery speeds.[31] Although the response/recovery time increases as the wavelength increases, the response/recovery speed still has certain advantages for sensors at RT.

For the composites, the addition of a small amount of BiOI has no obvious effect on the morphology of ZnO and hence has little effect on the diffusion process of NO_2 in the composites. The enhanced NO_2 sensitivity of composites can be explained as follows. First, the addition of BiOI induces more O_V defects, which is proved by the results of UV−vis absorption and XPS in Figure 3d,e. To further illustrate the

https://doi.org/10.1021/acssensors.2c01988
ACS Sens. 2022, 7, 3915−3922

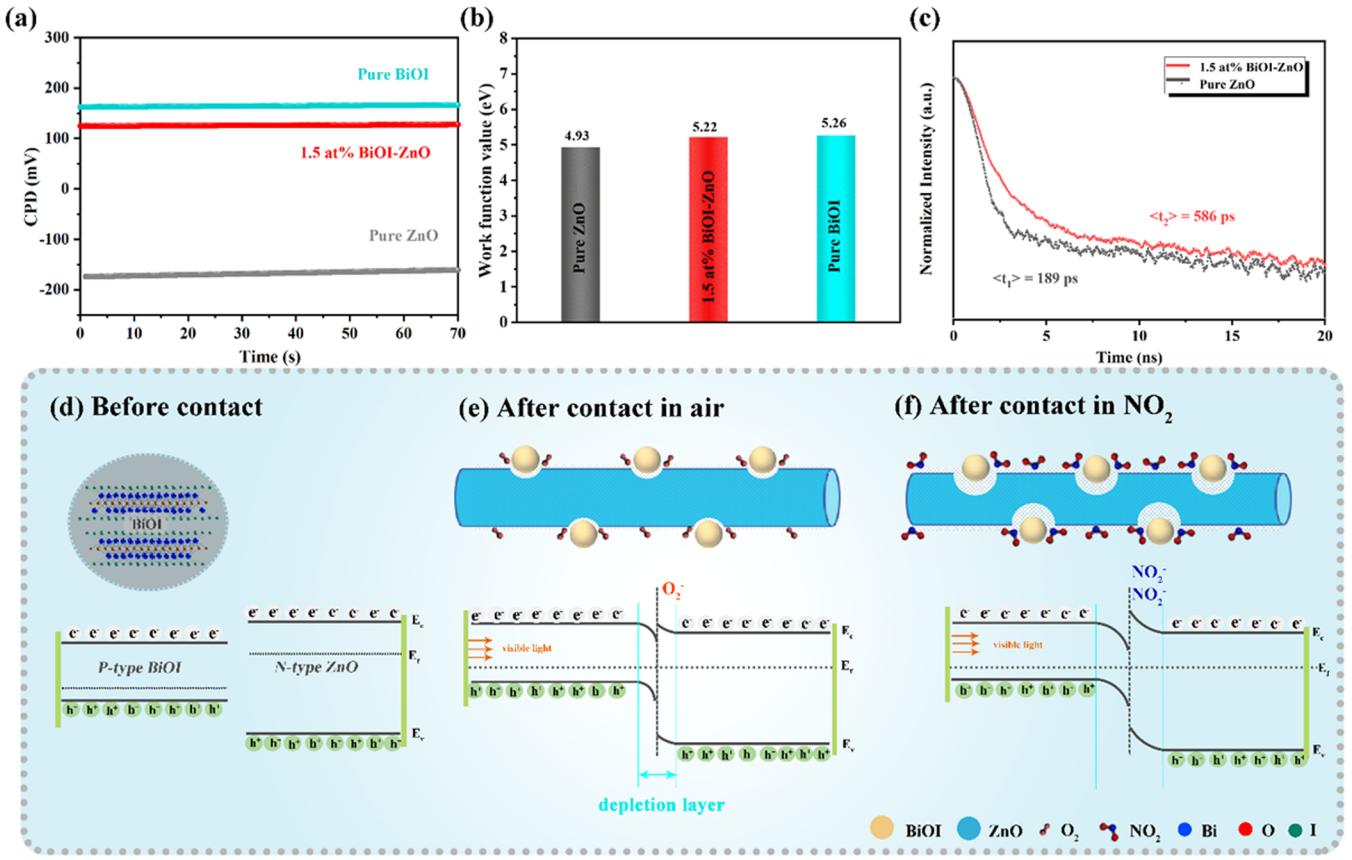

Figure 6. (a) Contact potential difference and (b) the corresponding work function of the samples. (c) TRPL decay curves. The energy level (d) before contact, (e) after contact in the air, and (f) after contact in NO_2.

role of O_V, the sensing properties were separately tested in pure N_2, simulated air (~20% O_2 and ~0% RH), and pure O_2, as shown in Figure S7. The base resistance in pure O_2 was the highest, which is attributed to the adsorption of O_2 on O_V according to eq 4. In pure N_2, since more reaction sites are occupied by NO_2 instead of O_2, the reaction in eq 5 dominates the whole process, leading to the highest response.

Second, the formed heterojunctions promote the sensing performance, even though they might also be not conducive to the electron transfer between grains and bring adverse effects on the response/recovery speed, as shown in Figure 5e,f. W_f values of ZnO and BiOI obtained by the Kelvin probe were 4.93 and 5.26 eV, respectively, as shown in Figure 6a,b. Therefore, when they contact, charge transfers across the interface due to the inconsistent Fermi level (E_f) to form heterojunctions. Eventually, E_f is aligned, and the W_f of the composite was about 5.22 eV between those of pure ZnO and BiOI. More importantly, the interfacial barrier (V) formed by the heterojunction modulates the resistance of the sensor as eq 8, which indirectly enhances the sensitivity of the sensor.[32]

$$R = R_0 \exp(qV/kT) \tag{8}$$

where R and R_0 are the resistances of the sensor. q, k, and T are, respectively, the electron charge, Boltzmann constant, and temperature.

For further investigating the role of heterojunctions, TRPL curves were performed, as shown in Figure 6c, related to the carriers' decay lifetime, which can well fit with biexponential functions (eq 9).

$$y = a_1 \exp(-t/\tau_1) + a_2 \exp(-t/\tau_2) + C \tag{9}$$

where the fast decay component τ_1 was attributed to the nonradiative recombination of free carriers, which was the major deactivation pathway, and the long decay component τ_2 came from the radiative recombination. The average decay time can be calculated as eq 10, and the results are displayed in Table S3.

$$\langle t \rangle = (a_1\tau_1^2 + a_2\tau_2^2)/(a_1\tau_1 + a_2\tau_2) \tag{10}$$

It was noted that $\langle t \rangle_{BiOI-ZnO}$ was higher than $\langle t \rangle_{ZnO}$, suggesting the faster charge transport speed and reduced recombination of photogenerated carriers. The results proved that the formed heterojunctions in the composites promoted the separation of photogenerated carriers and thus enhanced the catalytic activity of the surface.[33] The whole process is presented in Figure 6d–f.

Additionally, combined with the existing application of BiOI in the solar cell field, the $I-V$ curves of the sensor to various intensity lights under a low bias voltage are recorded in Figure S8. The short-circuit current (I_{sc}) and the open-circuit voltage (V_{oc}), as the fingerprint of the photovoltaic effect, increased with the increase of intensities due to the built-in electronic field at the interface between BiOI and ZnO.[34] This means that the effect of light on this BiOI–ZnO composite and its application in photovoltaic self-powered sensors is also an issue worthy of attention in future research.

https://doi.org/10.1021/acssensors.2c01988
ACS Sens. 2022, 7, 3915–3922

CONCLUSIONS

In this work, ZnO NRs were prepared by the facile hydrothermal method and combined with BiOI nanoparticles. The characterization of sensors was studied in detail, and a 1.5 atom % BiOI−ZnO-based sensor showed the best NO_2-sensing performance including sufficient responses, fast response/recovery time, lower detection limit, and excellent selectivity and repeatability under 520 nm light because of the increasing number of O_V and the prolonged carrier lifetime. Moreover, the gas-sensing mechanism has been further discussed using the adsorption model. Interestingly, the observed photovoltaic effect shows that the sensor deserves further research in terms of photovoltaic self-powered devices.

ASSOCIATED CONTENT

Supporting Information

The Supporting Information is available free of charge at https://pubs.acs.org/doi/10.1021/acssensors.2c01988.

Synthesis of ZnO, BiOI, and BiOI−ZnO; gas-sensing measurement; characterization; XRD patterns of pure BiOI and BiOI−ZnO; FTIR spectrum of pure BiOI; XPS results of Bi 4f and I 3d; *I*−*V* curves of ZnO, BiOI, and BiOI−ZnO under 520 nm light; response curves of pure ZnO and BiOI−ZnO under 365, 460, and 490 nm lights; gas-sensing properties of BiOI−ZnO under 520 nm light in N_2, dry air, and O_2; parameters of TRPL for ZnO and BiOI−ZnO (PDF)

AUTHOR INFORMATION

Corresponding Authors

Fengmin Liu − *State Key Laboratory of Integrated Optoelectronics, Key Laboratory of Advanced Gas Sensor, Jilin Province, College of Electronic Science and Engineering, Jilin University, Changchun 130012, China;* orcid.org/0000-0003-1523-2915; Email: liufm@jlu.edu.cn

Geyu Lu − *State Key Laboratory of Integrated Optoelectronics, Key Laboratory of Advanced Gas Sensor, Jilin Province, College of Electronic Science and Engineering, Jilin University, Changchun 130012, China; International Center of Future Science, Jilin University, Changchun 130012, China;* orcid.org/0000-0002-7428-2456; Email: lugy@jlu.edu.cn

Authors

Yueyue Li − *State Key Laboratory of Integrated Optoelectronics, Key Laboratory of Advanced Gas Sensor, Jilin Province, College of Electronic Science and Engineering, Jilin University, Changchun 130012, China*

Yuanzhen Liu − *State Key Laboratory of Integrated Optoelectronics, Key Laboratory of Advanced Gas Sensor, Jilin Province, College of Electronic Science and Engineering, Jilin University, Changchun 130012, China*

Yi Lu − *State Key Laboratory of Integrated Optoelectronics, Key Laboratory of Advanced Gas Sensor, Jilin Province, College of Electronic Science and Engineering, Jilin University, Changchun 130012, China*

Ziqi Liu − *State Key Laboratory of Integrated Optoelectronics, Key Laboratory of Advanced Gas Sensor, Jilin Province, College of Electronic Science and Engineering, Jilin University, Changchun 130012, China*

Chengming Sui − *State Key Laboratory of Integrated Optoelectronics, Key Laboratory of Advanced Gas Sensor, Jilin Province, College of Electronic Science and Engineering, Jilin University, Changchun 130012, China*

Yilin Wang − *State Key Laboratory of Integrated Optoelectronics, Key Laboratory of Advanced Gas Sensor, Jilin Province, College of Electronic Science and Engineering, Jilin University, Changchun 130012, China*

Lin Yang − *State Key Laboratory of Integrated Optoelectronics, Key Laboratory of Advanced Gas Sensor, Jilin Province, College of Electronic Science and Engineering, Jilin University, Changchun 130012, China*

Peng Sun − *State Key Laboratory of Integrated Optoelectronics, Key Laboratory of Advanced Gas Sensor, Jilin Province, College of Electronic Science and Engineering, Jilin University, Changchun 130012, China; International Center of Future Science, Jilin University, Changchun 130012, China;* orcid.org/0000-0002-9509-9431

Fangmeng Liu − *State Key Laboratory of Integrated Optoelectronics, Key Laboratory of Advanced Gas Sensor, Jilin Province, College of Electronic Science and Engineering, Jilin University, Changchun 130012, China; International Center of Future Science, Jilin University, Changchun 130012, China;* orcid.org/0000-0002-5555-5543

Complete contact information is available at: https://pubs.acs.org/10.1021/acssensors.2c01988

Notes

The authors declare no competing financial interest.

ACKNOWLEDGMENTS

This work was supported by the National Key Research and Development Program of China (No. 2021YFB3201301), the National Natural Science Foundation of China (Nos. 61871198, 62271225, 61831011, and 61833006), and Project on Industrial Innovation Capability of Jilin Province (No. 2020C048).

REFERENCES

(1) Ibrahim, M. F.; Hod, R.; Tajudin, M. A. B. A.; Mahiyuddin, W. R. W.; Nawi, A. M.; Sahani, M. Children's exposure to air pollution in a natural gas industrial area and their risk of hospital admission for respiratory diseases. *Environ. Res.* **2022**, *210*, No. 112966.

(2) de Prado-Bert, P.; Warembourg, C.; Dedele, A.; Heude, B.; Borras, E.; Sabido, E.; Aasvang, G. M.; Lepeule, J.; Wright, J.; Urquiza, J.; et al. Short- and medium-term air pollution exposure, plasmatic protein levels and blood pressure in children. *Environm. Res.* **2022**, *211*, No. 113109.

(3) Liang, D. H.; Shi, L. H.; Zhao, J. X.; Liu, P. F.; Sarnat, J. A.; Gao, S.; Schwartz, J.; Liu, Y.; Ebelt, S. T.; Scovronick, N.; et al. Urban Air Pollution May Enhance COVID-19 Case-Fatality and Mortality Rates in the United States. *Innovation* **2020**, *1*, No. 100047.

(4) Choi, M. S.; Kim, M. Y.; Mirzaei, A.; Kim, H.-S.; Kim, S.-I.; Baek, S.-H.; Chun, D. W.; Jin, C.; Lee, K. H. Selective, sensitive, and stable NO_2 gas sensor based on porous ZnO nanosheets. *Appl. Surf. Sci.* **2021**, *568*, No. 150910.

(5) Wang, H.; Bai, J.; Dai, M.; Liu, K.; Liu, Y.; Zhou, L.; Liu, F.; Liu, F.; Gao, Y.; Yan, X.; Geyu, L. Visible light activated excellent NO_2 sensing based on 2D/2D ZnO/g-C_3N_4 heterojunction composites. *Sens. Actuators, B* **2020**, *304*, No. 127287.

(6) Kim, J.-S.; Yoon, J.-W.; Hong, Y. J.; Kang, Y. C.; Abdel-Hady, F.; Wazzan, A. A.; Lee, J.-H. Highly sensitive and selective detection of ppb-level NO_2 using multi-shelled WO_3 yolk-shell spheres. *Sens. Actuators, B* **2016**, *229*, 561−569.

(7) Mirzaei, A.; Janghorban, K.; Hashemi, B.; Bonyani, M.; Leonardi, S. G.; Neri, G. A novel gas sensor based on Ag/Fe_2O_3 core-shell nanocomposites. *Ceram. Int.* **2016**, *42*, 18974−18982.

(8) Zhang, Q. P.; Chen, C. X.; Liu, Y. T.; Xu, M.; Xie, G. Z.; Tai, H. L.; Du, X. S.; Jiang, Y. D.; Su, Y. J. Room-temperature light-activated chemical sensors for gas monitoring and applications: a review. *J. Phys. D: Appl. Phys.* **2022**, *55*, No. 213001.
(9) Zhu, L.; Zeng, W. Room-temperature gas sensing of ZnO-based gas sensor: A review. *Sens. Actuators, A* **2017**, *267*, 242−261.
(10) Zhang, J.; Liu, X. H.; Neri, G.; Pinna, N. Nanostructured Materials for Room-Temperature Gas Sensors. *Adv. Mater.* **2016**, *28*, 795−831.
(11) Liu, A.; Lv, S.; Jiang, L.; Liu, F.; Zhao, L.; Wang, J.; Hu, X.; Yang, Z.; He, J.; Wang, C.; et al. The gas sensor utilizing polyaniline/MoS_2 nanosheets/ SnO_2 nanotubes for the room temperature detection of ammonia. *Sens. Actuators, B* **2021**, *332*, No. 129444.
(12) Karpe, S. B.; Bang, A. D.; Adhyapak, D. P.; V Adhyapak, P. Fabrication of high sensitive proto-type NO_x sensor based on Pd nanoparticles loaded on WO_3. *Sens. Actuators, B* **2022**, *354*, No. 131203.
(13) Liu, Z.; Chen, J.; Lv, H.; Wang, S.; Fan, J.; Kan, K.; Pan, K.; Shi, K. Monodispersed ultra-thin BiOCl nanosheets with (110) facets exposed in situ self-assembled on reduced graphene oxide to enhance NO_2 sensing performance at room temperature. *Sens. Actuators, B* **2022**, *351*, No. 130932.
(14) Wang, H. T.; Dai, M.; Li, Y. Y.; Bai, J. H.; Liu, Y. Y.; Li, Y.; Wang, C. C.; Liu, F. M.; Lu, G. Y. The influence of different ZnO nanostructures on NO_2 sensing performance. *Sens. Actuators, B* **2021**, *329*, No. 129145.
(15) Chen, J. F.; Hu, C.; Deng, Z.; Gong, X. P.; Su, Y.; Yang, Q.; Zhong, J. B.; Li, J. Z.; Duan, R. Insight into visible light-driven photocatalytic performance of direct Z-scheme Bi_2WO_6/BiOI composites constructed in-situ. *Chem. Phys. Lett.* **2019**, *716*, 134−141.
(16) Ouyang, W. X.; Chen, J. X.; He, J. H.; Fang, X. S. Improved Photoelectric Performance of UV Photodetector Based on ZnO Nanoparticle-Decorated BiOCl Nanosheet Arrays onto PDMS Substrate: The Heterojunction and $Ti_3C_2T_x$ MXene Conduction Layer. *Adv. Electron. Mater.* **2020**, *6*, No. 2000168.
(17) Wang, L. Y.; Daoud, W. A. BiOI/TiO_2-nanorod array heterojunction solar cell: Growth, charge transport kinetics and photoelectrochemical properties. *Appl. Surf. Sci.* **2015**, *324*, 532−537.
(18) Natarajan, K.; Bajaj, H. C.; Tayade, R. J. Photocatalytic efficiency of bismuth oxyhalide (Br, Cl and I) nanoplates for RhB dye degradation under LED irradiation. *J. Ind. Eng. Chem.* **2016**, *34*, 146−156.
(19) Yueyue, L.; Siqi, S.; Yilin, W.; Fengmin, L.; Hongtao, W.; Jihao, B.; Min, L.; Geyu, L. $CsPbBr_3$ quantum dots enhanced ZnO sensing to NO_2 at room temperature. *Sens. Actuators, B* **2022**, *368*, No. 132189.
(20) Xiao, W. S.; Su, Y.; Luo, J.; Jiang, L.; Wu, X. J.; Liu, Z. P.; Pang, H. J.; Zhang, Q. L.; Zhang, P. Flower-like hierarchical architecture of BiOI/ZnO p-n junction composites with high-efficient visible-light photodegradation activities. *Solid State Sci.* **2020**, *108*, No. 106432.
(21) Liu, J.; Zou, S.; Lou, B.; Chen, C.; Xiao, L.; Fan, J. Interfacial Electronic Interaction Induced Engineering of ZnO-BiOI Heterostructures for Efficient Visible-Light Photocatalysis. *Inorg. Chem.* **2019**, *58*, 8525−8532.
(22) Umar, A.; Kim, B. K.; Kim, J. J.; Hahn, Y. B. Optical and electrical properties of ZnO nanowires grown on aluminium foil by non-catalytic thermal evaporation. *Nanotechnology* **2007**, *18*, No. 175606.
(23) Mohan, L.; Sisupalan, N.; Ponnusamy, K.; Sadagopalan, S. One Step Synthesis and Characterization of ZnO-ZnSe Heterostructures by Chemical Precipitation and Its Solar Photocatalytic Activity. *J. Inorg. Organomet. Polym.* **2020**, *30*, 2626−2632.
(24) Fang, S. S.; Lu, M.; Zhou, M.; Li, Z. Y.; Xu, S.; Peng, Y. Y.; Li, Q. C.; Lu, D. Y. Facile Synthesis and Characterization of Novel CdS/BiOI Heterojunctions with Enhanced Visible-Light Photocatalytic Performances. *Acta Phys. Pol., A* **2017**, *131*, 263−270.
(25) Muthukumaran, S.; Gopalakrishnan, R. Structural, FTIR and photoluminescence studies of Cu doped ZnO nanopowders by co-precipitation method. *Opt. Mater.* **2012**, *34*, 1946−1953.
(26) Xu, J. J.; Hu, Y. M.; Zeng, C.; Zhang, Y. H.; Huang, H. W. Polypyrrole decorated BiOI nanosheets: Efficient photocatalytic activity for treating diverse contaminants and the critical role of bifunctional polypyrrole. *J. Colloid Interface Sci.* **2017**, *505*, 719−727.
(27) Chen, C. X.; Zhang, Q. P.; Xie, G. Z.; Yao, M. L.; Pan, H.; Du, H. F.; Tai, H. L.; Du, X. S.; Su, Y. J. Enhancing visible light-activated NO_2 sensing properties of Au NPs decorated ZnO nanorods by localized surface plasmon resonance and oxygen vacancies. *Mater. Res. Express* **2020**, *7*, No. 015924.
(28) Kong, D. H.; Han, J. Y.; Gao, Y. B.; Gao, Y.; Zhou, W. R.; Liu, G. N.; Lu, G. Y. Lower coordination Co_3O_4 mesoporous hierarchical microspheres for comprehensive sensitization of triethylamine vapor sensor. *J. Hazard. Mater.* **2022**, *430*, No. 128469.
(29) Wang, Z. Y.; Gao, S.; Fei, T.; Liu, S.; Zhang, T. Construction of ZnO/SnO_2 Heterostructure on Reduced Graphene Oxide for Enhanced Nitrogen Dioxide Sensitive Performances at Room Temperature. *ACS Sens.* **2019**, *4*, 2048−2057.
(30) Wongrat, E.; Pimpang, P.; Choopun, S. Comparative study of ethanol sensor based on gold nanoparticles: ZnO nanostructure and gold: ZnO nanostructure. *Appl. Surf. Sci.* **2009**, *256*, 968−971.
(31) Huang, Y. F.; Jiao, W. C.; Chu, Z. M.; Nie, X. M.; Wang, R. G.; He, X. D. SnS_2 Quantum Dot-Based Optoelectronic Flexible Sensors for Ultrasensitive Detection of NO_2 Down to 1 ppb. *Acs Appl. Mater. Interfaces* **2020**, *12*, 25178−25188.
(32) Miller, D. R.; Akbar, S. A.; Morris, P. A. Nanoscale metal oxide-based heterojunctions for gas sensing: A review. *Sens. Actuators, B* **2014**, *204*, 250−272.
(33) Wang, J.; Tang, L.; Zeng, G.; Deng, Y.; Dong, H.; Liu, Y.; Wang, L.; Peng, B.; Zhang, C.; Chen, F. 0D/2D interface engineering of carbon quantum dots modified Bi_2WO_6 ultrathin nanosheets with enhanced photoactivity for full spectrum light utilization and mechanism insight. *Appl. Catal., B* **2018**, *222*, 115−123.
(34) Niu, Y.; Zeng, J.; Liu, X.; Li, J.; Wang, Q.; Li, H.; Rooij, N. F.; Wang, Y.; Zhou, G. A Photovoltaic Self-Powered Gas Sensor Based on All-Dry Transferred MoS_2 /GaSe Heterojunction for ppb-Level NO_2 Sensing at Room Temperature. *Adv. Sci.* **2021**, *8*, No. e2100472.

https://doi.org/10.1021/acssensors.2c01988
ACS Sens. 2022, 7, 3915−3922